Theor Chem Acc (2011) 129:625–630
DOI 10.1007/s00214-011-0910-3

REGULAR ARTICLE

Attractive interaction between transition-metal atom impurities and vacancies in graphene: a first-principles study

A. V. Krasheninnikov · R. M. Nieminen

Received: 15 October 2010 / Accepted: 11 February 2011 / Published online: 12 March 2011

Abstract We present a density functional theory study of transition metal adatoms on a graphene sheet with vacancy-type defects. We calculate the strain fields near the defects and demonstrate that the strain fields around these defects reach far into the unperturbed hexagonal network and that metal atoms have a high affinity to the non-perfect and strained regions of graphene. Metal atoms are therefore attracted by the reconstructed defects. The increased reactivity of the strained graphene makes it possible to attach metal atoms much more firmly than to pristine graphene and supplies a tool for tailoring the electronic structure of graphene. Finally, we analyze the electronic band structure of graphene with defects and show that some defects open a semiconductor gap in graphene, which may be important for carbon-based nanoelectronics.

Keywords Graphene · Point defects · Electronic band structure · Strain fields

1 Introduction

Graphene [1], a promising candidate for next generation electronics, is a novel two-dimensional (2D) material made from carbon with a honeycomb-like arrangement of the atoms [2]. The electronic and mechanical properties of graphene samples with high perfection of the atomic lattice are exceptional [1]. For example, semimetallic graphene has the linear dispersion relation and high mobility of charge carriers, [3] while its Young's modulus is about 1 TPa, [4] the highest among known.

However, structural defects [5], which may appear during growth or processing, should deteriorate graphene properties and the performance of graphene-based devices. At the same time, deviations from perfection can also be useful in some applications, as they make it possible to tailor the local properties of graphene and to achieve new functionalities, for example, by opening a semiconducting gap [6, 7] required for the operation of graphene-based transistors.

Foreign atoms can also be incorporated into graphene as substitutional impurities forming extrinsic defects. In this case, the impurity atom replaces one or two carbon atoms. Boron or nitrogen serve as the natural dopants in carbon nanostructures [8–13] since they have one electron less or more, respectively, but roughly the same atomic radius. This mechanism of graphene doping has received particular attention, along with those [14, 15] based on the adsorption of organic molecules as well as metal atoms and clusters.

Much larger atoms such as transition metal (TM) impurities [16–18] can be incorporated into the atomic network as well, or added as adatoms. This issue has received lots of attention in the context of the unconventional Kondo effect in graphene and spintronics [19–22], its doping [3] and possible catalysis [23]. Furthermore, the precise knowledge of the details of TM–sp^2-carbon interaction is important for understanding carbon nanotube growth [24], fuel cell properties [25], and the role of

Dedicated to Professor Pekka Pyykkö on the occasion of his 70th birthday and published as part of the Pyykkö Festschrift Issue.

A. V. Krasheninnikov · R. M. Nieminen
Department of Applied Physics, Aalto University,
P.O. Box 1100, Helsinki 00076, Finland

A. V. Krasheninnikov (✉)
Department of Physics, University of Helsinki,
P.O. Box 43, Helsinki 00014, Finland
e-mail: akrashen@acclab.helsinki.fi

implanted magnetic atoms such as Fe in the development of magnetic order in carbon materials [26].

Earlier experimental [17, 27] and theoretical studies [16–18, 28, 29] demonstrated that the preferred way to incorporate TM impurities in graphene is to attach them to vacancies. Substitutional dopants are expected to be very stable due to strong covalent bonding of TM atoms to the host carbon matrix. The binding energies for the TM-vacancy complexes were reported to be in the range of 2–8 eV, [16, 28, 29] indicating strong bonding, and pointing to a possible use of such structures in catalysis. It was also suggested [16] to use spatially localized electron irradiation to create defects with atomic precision and then, by making co-deposited metal atoms mobile at elevated temperatures, to pin the atoms at the defects. This idea was experimentally implemented [30] later on for Fe, Co, and Mo atoms.

However, substitutional impurities are strong scatterers of electronic states in graphene [3], and alternative ways for implementing spatially localized doping has been searched for. Recent experiments [17] on W atoms on defected graphite indicated that the bonding may be more complicated than the simple model of substitutional impurities predicts. The strong bonding (e.g., 8.6 or 8.9 eV for a tungsten atom trapped in a single or double vacancy, respectively) was inconsistent with the thermal and possibly irradiation-induced migration observed in the experiments. To explain the contradiction, it was suggested [17] that reconstructed point defects in graphene created by electron irradiation and annealing can also pin the adatoms. It was shown that the strain field around a reconstructed di-vacancy (the so-called 555-777 defects) reaches far into the unperturbed hexagonal network and that metal atoms have a high affinity to the non-perfect and strained regions of graphene. Metal atoms are therefore attracted by reconstructed defects and bonded with energies of the order of 2 eV.

In this article, we focus on the strain fields near all reconstructed vacancy-type defects and on the mechanism of adatom-defect interaction. By employing first-principles simulation, we visualize the strain fields near vacancy-type defects in graphene and demonstrate that such defects create areas with a size of 2–3 nm where adatoms are attracted to the defects. We further calculate the adsorption energy as a function of mechanical strain for several TM adatoms and, finally, we present the electronic structure of the most important vacancy-type defects.

2 Computational details

The density functional theory (DFT) *ab initio* calculations were carried out with the VASP simulation package [31] using projector augmented wave (PAW) potentials [32] to describe core electrons, and the Generalized Gradient Approximation of Perdew, Burke, and Ernzernhof (PBE) [33] for exchange and correlation. The kinetic energy cutoff for the plane waves was set to 400 eV, and all structures were relaxed until atomic forces were below 0.01 eV/Å. Increasing the cutoff energy up to 600 eV changed the bonding energies by less than 10 meV. The sampling scheme of Monkhorts-Pack [34] with up to $9 \times 9 \times 1$ k-points meshes was used to integrate over the Brillouin zone.

Graphene was modeled as a supercell composed from 10×10 graphene unit cells so that the initial structure, in which the defects were introduced, consisted of 200 carbon atoms. The unit cell is shown in Fig. 1. Besides, to study the effects of uniaxial strain on the adsorption energy of TM adatoms, a rectangular simulation cell composed from 96 atoms was used.

3 Results

3.1 Strain fields near vacancy-type defects

The most prolific defects produced by energetic electrons in graphene are vacancies [35]. Single vacancies (SV) in graphene [36, 37] and nanotubes [38, 39] undergo a Jahn-Teller distortion, which leads to the saturation of two of the three dangling bonds toward the missing atom. One dangling bond always remains due to geometrical reasons. It is intuitively clear that due to the presence of an under-coordinated carbon atom, and a lower displacement threshold for this atom [40], SV should be quickly transformed to a di-vacancy (DV), which can also be referred to as a 5-8-5 defect. The DV also reconstructs, so that two new weak bonds are formed, lowering the energy of the system.

Besides, at elevated temperatures (over 200 °C), SVs also transform to DVs due to SV migration and coalescence [41]. DVs undergo further transformations to 555-777 [42] and 5555-6-7777 defects by bond rotations, as this process lowers the total energy of the system by more than 1 eV per defect. The atomic structures of these defects are presented in Fig. 1. Note that in panels (b–d) the same number of carbon atoms (two) are missing.

Previous simulations [17] showed that the binding (adsorption) energy (negatively defined) near a 555-777 defect decreases, as shown in Fig. 2 and that the drop in energy can be explained by a combination of two effects: strain fields near the defects and the decrease in the adsorption energy of the adatom on top of strained bonds. All of these gives rise to the effective attraction of the adatoms by the defects.

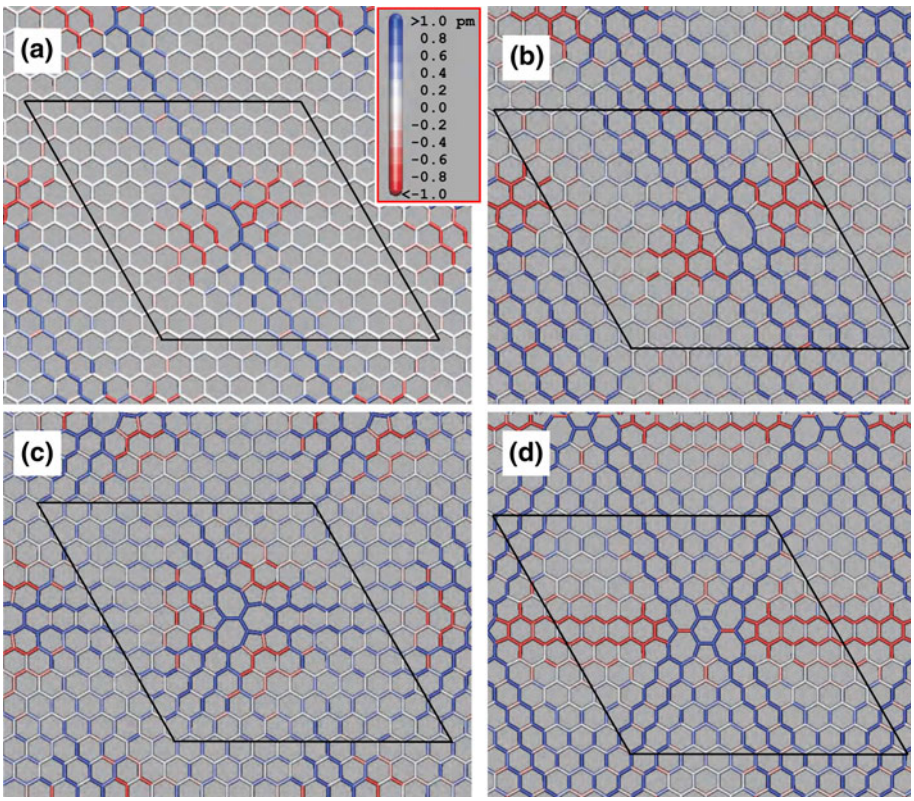

Fig. 1 Atomic structures of a single vacancy (**a**), di-vacancy [5-8-5 defect] (**b**), and the reconstructed di-vacancy defect including the 555-777 (**c**) and 5555-6-7777 defect (**d**). The latter defects were obtained by rotating one of the carbon bonds in the di-vacancy defect. Such defects have lower energies as the parent structure shown in panel (**b**). The bonds are colored according to an increase (*blue*) or decrease (*red*) in the bond length (given in picometers). The bonds close to pentagons are contracted, but most C–C bonds are stretched. The *black lines* outline the simulation supercell (10 × 10 graphene unit). It is evident that the strain fields extend for at least 2 nm away from the defect

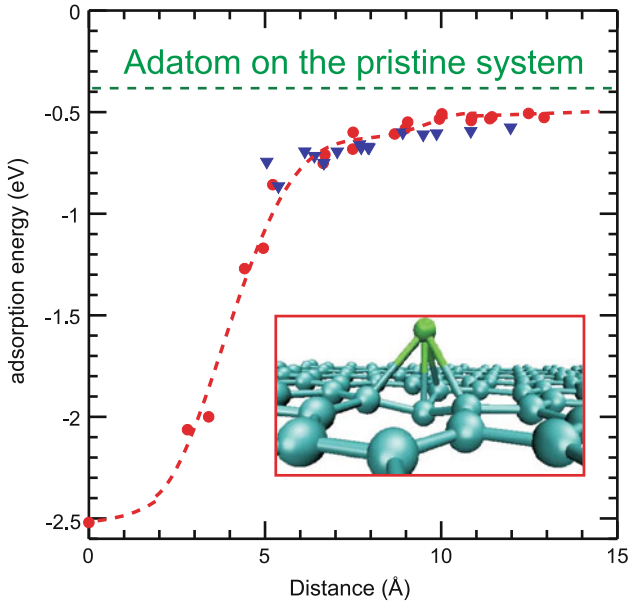

Fig. 2 Adsorption energy of a W adatom near the 555-777 defect as a function of separation between the adatom and the middle of the defect (the central atom in Fig. 1c shared among the three heptagons). The *blue triangles* and *red circles* correspond to the bridge and middle-of-hexagon positions of the adatom. The *inset* shows the position of the adatom in the lowest energy configuration

In order to better understand the mechanism of the attractive interaction, we calculated strain fields near the SV, DV, and related defects, Fig. 1. The strain fields were visualized as the difference between the bond lengths in the system with a defect and that in the pristine sheet. It is evident that all vacancy-type defects give rise to strain fields in their vicinity, with the range of at least 2–3 nm or possibly even more (larger than the supercell). Most C–C bonds are stretched, but the bonds close to pentagons are contracted, as graphene is an elastic material with a finite value of Poisson ratio [43].

3.2 Strain fields near metal adatoms on pristine graphene

As W adatoms on graphene have been used in recent experiments [17], we calculated the strain fields near W adatoms on pristine graphene. The existence of a strain field of opposite sign (with regard to vacancy-type defect) could have explained the attractive interaction between vacancies and adatoms. However, in a two-dimensional system, the weakly bonded W adatom does not create a long-range strain field of the opposite sign in the carbon network, Fig. 3b, c, and the conventional mechanism of vacancy-interstitial attraction as in 3D bulk systems does not work.

We did not find any long-range strain fields near other adatoms we studied (W, Cr, Mo). This is an expected result, as adatom binding energy to graphene sheet is relatively small, about 0.5 eV, and the adatom is well outside the plane.

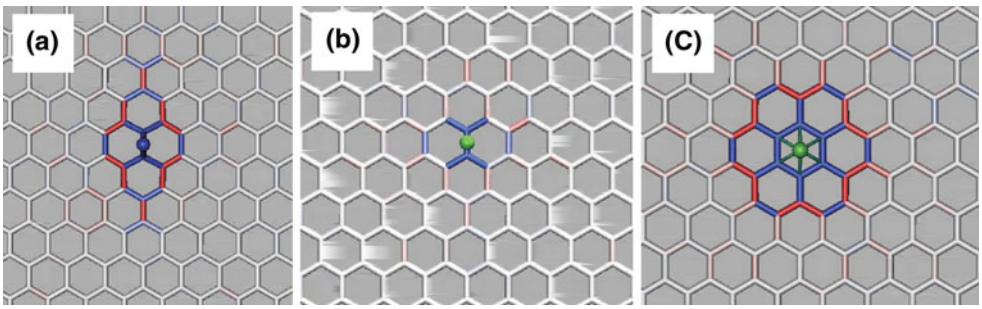

Fig. 3 Atomic structure of the graphene sheet with adatoms and strain fields near the adatom. **a** Carbon adatom. W adatom in the bridge (**b**) and middle-of-hexagon (**c**) positions. The bonds are colored according to the increase (*blue*) or decrease (*red*) in the bond length (given in picometers) with regard to the pristine system. It is evident that there is no considerable long-ranged strain field. The coloring scheme is the same as in the case of the vacancy-type defects shown in Fig. 1. The balls represent the adatoms

We also calculated the strain fields near carbon adatoms. Interestingly enough, even carbon adatoms which bind relatively strongly to graphene [44] and nanotubes [45] with energies 1–3 eV also give rise to changes in the bond lengths between the nearest neighbors of the adatom only, so that no long-range strain effect is present.

3.3 Adsorption energy of metal adatoms on strained graphene

To understand the reason for the attractive interaction, we first calculated the adsorption energy of the W adatom on the strained graphene sheet. A biaxial strain of 1% (respectively 2%) lowers the energy for the middle-of-hexagon position from initially −0.38 to −0.54 (− 0.69) eV and for the bridge position from −0.45 to −0.52 (−0.59) eV, respectively.

We also studied the adsorption for a more realistic case, corresponding to uniaxial mechanical strain. We calculated the decrease in the adsorption energy as a function of uniaxial strain in the armchair and zigzag directions, as sketched in the inset in Fig. 4 for W, Mo, and Cr adatoms. As evident from Fig. 4, mechanical strain always results in a stronger bonding.

The drop in energy and stronger bonding can be associated with a smaller saturation of the C–C bonds under strain, so that more electron density is available for making a new bond with the adatom. The energy decrease was larger when strain was applied in the zigzag direction when compared to the armchair diretion. Graphene is an anisotropic material, so that hexagons are deformed in slightly different ways. The effective coordination of the adatoms changes, as the symmetry (for the position of the adatom in the middle of the hexagon) is broken. When stress is applied in the zigzag direction, the shortest bonds connect the adatom with four C atoms, while for the armchair direction only with two atoms. This may explain why the drop in the adsorption energy is larger for the stress applied in the zigzag direction.

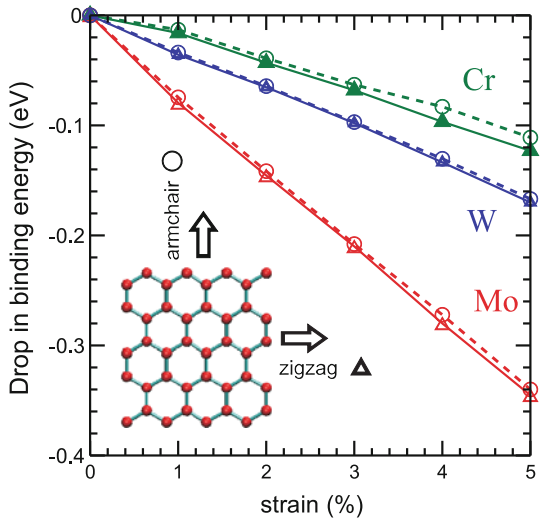

Fig. 4 Decrease in the binding (adsorption) energy of W, Cr, and Mo adatoms in the middle-of-hexagon configuration as a function of uniaxial mechanical strain in graphene. The system was strained along the armchair (*circles*) and zigzag (*triangles*) directions. The *inset* schematically shows strain directions

The observed energy gradient comes from a combination of the strain field and electronic effects. This observation points toward possible applications of graphene ribbons as strain sensors, as a drop in adsorption energy should increase the number of adsorbed species and thus affect the current through graphene ribbon [46]. The attractive interaction between the adatoms and defects is different from the known phenomenon of long-range interactions of adatoms on metals [47], graphite [48], or carbon nanotubes [49] which is mediated by purely electronic effects [50].

3.4 Electronic structure of vacancy-type defects

As the effects of point defects and impurities on the electronic structure of graphene presents considerable interest in the context of defect-mediated engineering of graphene

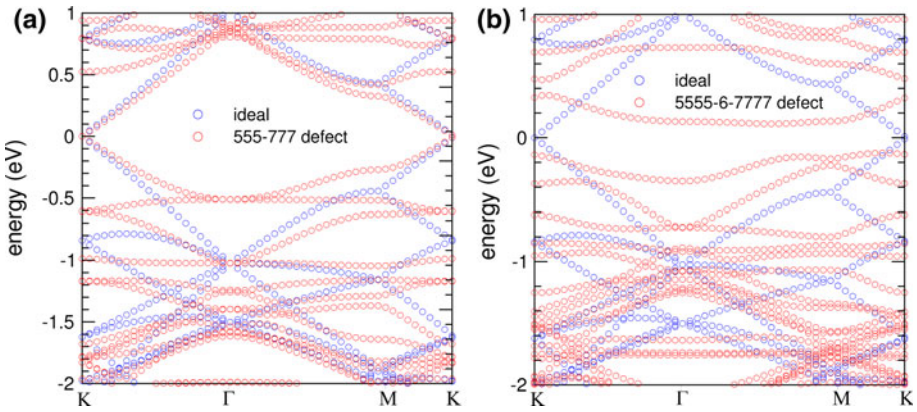

Fig. 5 Band structure of graphene 200-atom supercell with a 555-777 defect (**a**) and 5555-6-7777 defect (**b**). Note that for the 5555-6-7777 defect a gap about 0.3 is open. Zero energy corresponds to the position of the Fermi level in pristine graphene

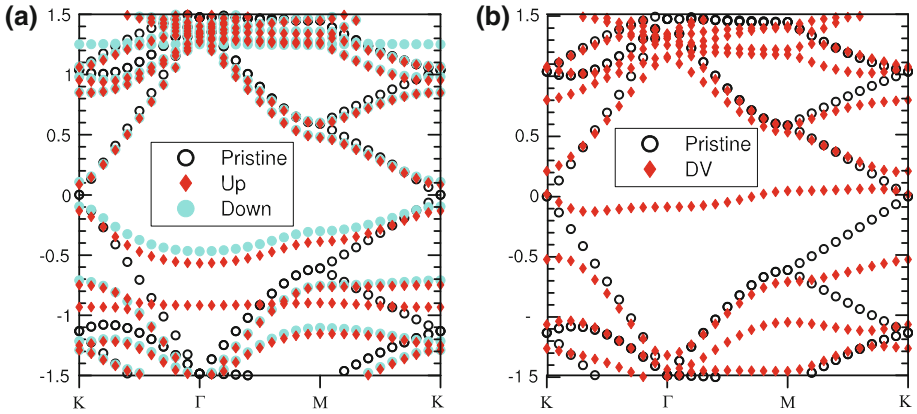

Fig. 6 Band structure of graphene 98-atom supercell with a single vacancy (**a**) and double vacancy defect (**b**)

electronic properties, we also calculated the band structure of graphene with the most stable vacancy-type defects, 555-777 and 5555-6-7777 configurations. For the sake of comparison, we also present here the band structures of SV and DV, although these defects are less stable than the 555-777 and 5555-6-7777 defects.

The band structure of a 200 atom supercell with a 555-777 defect is presented in Fig. 5a. It is evident that, although the defect gives rise to new localized states below the Fermi level (0.5 eV), it does not alter the electronic structure of graphene sheet at the Fermi level. Thus, one can expect that a TM atom-555-777 complex will be a weaker scattering center than the substitutional impurity, and thus the preferable way to incorporate TM atoms into the system.

The situation is quite different in the case of the 5555-6-7777 defect. A gap of more than 0.3 eV is opened at the Fermi level. The gap is much larger than that for SV and DV, about 0.1 eV, Fig. 6, which agrees with the previously published results [51]. Besides, as mentioned above, the non-reconstructed SV and DV are less stable than the reconstructed defects, so that their probability to exist is smaller. Our results [7] indicate that a gap is always opened near complicated vacancy-type defects in graphene, when rotated hexagons, Fig. 1d are embedded into graphene through non-hexagonal rings (pentagons and heptagons). This result may be important for nanoelectronics, and spatially localized electron or ion irradiation [35, 52–56] can be used to produce such areas.

4 Conclusions

To conclude, we studied the details of the attractive interaction between p-vacancy-type point defects in graphene and transition metal adatoms. We showed that the 555-777-type reconstructed vacancies, which are the predominant defects in a wide temperature range, are efficient trapping centers for metal adatoms. Metal atoms migrating on graphene are attracted by these defects at distances in the nano-metre range. The interaction between defects in graphene and metal atoms is different from the known mechanisms of strain fields and electronic effects in bulk systems and on their surfaces, and originates from an interplay of local strain in the atomic network, created by the defect, and electronic adsorption effects. The trapping of metal atoms in strained areas and at defects in graphene may be used for engineering the local electronic and magnetic structure of graphene and its doping by the controlled production of defects. Finally, we analyzed the

band structure of graphene with defects and show that some defects open a semiconductor gap in graphene, which may be important for the development of carbon-based nanoelectronics.

Acknowledgments We acknowledge the valuable discussions with Pekka Pyykkö concerning transition metal-carbon bonding and salute his long-standing, remarkable contributions to electronic-structure theory and calculations in general. We also thank F. Banhart for useful discussions. This work was supported by The Academy of Finland through Centres of Excellence and other projects. The Finnish IT Center for Science provided generous grants of computer time.

References

1. Geim AK, Novoselov KS (2007) Nature Mater 6:183–191
2. Meyer JC, Geim AK, Katsnelson MI, Novoselov KS, Booth TJ, Roth S (2007) Nature 446:60–63
3. Castro Neto AH, Guinea F, Peres NMR, Novoselov KS, Geim AK (2009) Rev Mod Phys 81:109–162
4. Lee C, Wei X, Kysar JW, Hone J (2008) Sci Agric 321:385–388
5. Banhart F, Kotakoski J, Krasheninnikov AV (2011) ACS Nano 5:26–41
6. Appelhans DJ, Lin Z, Lusk MT (2010) Phys Rev B 82:073410
7. Kotakoski J, Krasheninnikov AV, Kaiser U, Meyer JC (2011) Phys Rev Lett (in press)
8. Wang X, Li X, Zhang L, Yoon Y, Weber PK, Wang H, Guo J, Dai H (2009) Science 324:768–771
9. Reddy ALM, Srivastava A, Gowda SR, Gullapalli H, Dubey M, Ajayan PM (2010) ACS Nano 4:6337–6342
10. Biel B, Blase X, Triozon F, Roche S (2009) Phys Rev Lett 102:096803
11. Zheng XH, Rungger I, Zeng Z, Sanvito S (2009) Phys Rev B 80:235426
12. Dutta S, Manna AK, Pati SK (2009) Phys Rev Lett 102:096601
13. Krivanek OL, Chisholm MF, Nicolosi V, Pennycook TJ, Corbin GJ, Dellby N, Murfitt MF, Own CS, Szilagyi ZS, Oxley MP, Pantelides ST, Pennycook SJ (2010) Nature 464:571–574
14. Pinto H, Jones R, Goss J, Briddon PR (2010) Phys Status Solidi (a) 207:2131–2136
15. Subrahmanyam K, Manna AK, Pati SK, Rao CNR (2010) Chem Phys Lett 497:70–75
16. Krasheninnikov AV, Lehtinen PO, Foster AS, Pyykkö P, Nieminen RM (2009) Phys Rev Lett 102:126807
17. Cretu O, Krasheninnikov AV, Rodriguez-Manzo JA, Sun L, Nieminen R, Banhart F (2010) Phys Rev Lett 105:196102
18. Zhang W, Sun L, Xu Z, Krasheninnikov AV, Huai P, Zhu Z, Banhart F (2010) Phys Rev B 81:125425
19. Hentschel M, Guinea F (2007) Phys Rev B 76:115407
20. Sengupta K, Baskaran G (2008) Phys Rev B 77:045417
21. Dóra B, Thalmeier P (2007) Phys Rev B 76:115435
22. Shytov AV, Katsnelson MI, Levitov LS (2007) Phys Rev Lett 99:236801
23. Bittencourt C, Felten A, Douhard B, Colomer J-F, Van Tendeloo G, Drube W, Ghijsen J, Pireaux J-J (2007) Surf Sci 601:2800–2804
24. Yazyev OV, Pasquarello A (2008) Phys Rev Lett 100:156102
25. Che G, Lakshmi BB, Fisher ER, Martin CR (1998) Nature 393:346–349
26. Sielemann R, Kobayashi Y, Yoshida Y, Gunnlaugsson HP, Weyer G (2008) Phys Rev Lett 101:137206
27. Gan Y, Sun L, Banhart F (2008) Small 4:587–591
28. Santos EJG, Ayuela A, Fagan SB, Mendes Filho J, Azevedo DL, Souza Filho AG, Sánchez-Portal D (2008) Phys Rev B 78:195420
29. Santos EJG, Ayuela A, Sánchez-Portal D (2010) New J Phys 12:053012
30. Rodriguez-Manzo JA, Cretu O, Banhart F (2010) ACS Nano 4:3422–3428
31. Kresse G, Furthmüller J (1996) Comp Mat Sci 6:15
32. Blöchl PE (1994) Phys Rev B 50:17953–17979
33. Perdew JP, Burke K, Ernzerhof M (1996) Phys Rev Lett 77:3865–3868
34. Monkhorst HJ, Pack JD (1976) Phys Rev B 13:5188
35. Krasheninnikov AV, Banhart F (2007) Nature Mater 6:723–733
36. Lehtinen PO, Foster AS, Ma Y, Krasheninnikov AV, Nieminen RM (2004) Phys Rev Lett 93:187202
37. El-Barbary AA, Telling RH, Ewels CP, Heggie MI, Briddon PR (2003) Phys Rev B 68:144107
38. Krasheninnikov AV, Nordlund K, Sirviö M, Salonen E, Keinonen J (2001) Phys Rev B 63:245405
39. Krasheninnikov AV (2001) Sol Stat Comm 118:361–365
40. Krasheninnikov AV, Banhart F, Li JX, Foster AS, Nieminen R (2005) Phys Rev B 72:125428
41. Krasheninnikov AV, Lehtinen PO, Foster AS, Nieminen RM (2006) Chem Phys Lett 418:132–136
42. Lee G, Wang CZ, Yoon E, Hwang N, Kim D, Ho KM (2005) Phys Rev Lett 95:205501
43. Scarpa F, Adhikari S, Phani AS (2010) Nanotechnology 20:065709
44. Lehtinen PO, Foster AS, Ayuela A, Krasheninnikov A, Nordlund K, Nieminen RM (2003) Phys Rev Lett 91:017202
45. Krasheninnikov AV, Nordlund K, Lehtinen PO, Foster AS, Ayuela A, Nieminen RM (2004) Carbon 42:1021–1025
46. Schedin F, Geim AK, Morozov SV, Hill EW, Blake P, Katsnelson MI, Novoselov KS (2007) Nature Mater 6:652–655
47. Repp J, Moresco F, Meyer G, Rieder K-H (2000) Phys Rev Lett 85:2981–2984
48. Hornekær L, Rauls E, Xu W, Šljivančanin Ž, Otero R, Stensgaard I, Lægsgaard E, Hammer B, Besenbacher F (2006) Phys Rev Lett 97:186102
49. Buchs G, Krasheninnikov AV, Ruffieux P, Gröning P, Foster AS, Nieminen RM, Gröning O (2007) New J Phys 9:275–287
50. Cheianov VV, Fal'ko VI (2006) Phys Rev Lett 97:226801
51. Santos EJG, Sánchez-Portal D, Ayuela A (2010) Phys Rev B 81:125433
52. Krasheninnikov AV, Miyamoto Y, Tománek D (2007) Phys Rev Lett 99:016104
53. Compagnini G, Giannazzo F, Sonde S, Raineri V, Rimini E (2009) Carbon 47:3201–3207
54. Åström JA, Krasheninnikov AV, Nordlund K (2004) Phys Rev Lett 93:215503, ibid. 94, 029902(E) (2005)
55. Lemme MC, Bell DC, Williams JR, Stern LA, Baugher BWH, Jarillo-Herrero P, Marcus CM (2009) ACS Nano 3:2674–2676
56. Krasheninnikov AV, Nordlund K (2010) J Appl Phys 107:071301